

TECHNICAL ARTICLE

Performance Analysis of a PV Powered Variable Speed DC Fridge Integrated with PCM for Weak/Off-Grid Setting Areas

James Riffat, Cagri Kutlu, Emmanuel Tapia Brito, Yuehong Su and Saffa Riffat

This paper investigates the transient performance of a DC compressor fridge incorporated with Phase Change Material (PCM) for weak/off-grid setting regions. A photovoltaics (PV) module is directly connected to the DC compressor without use of batteries and inverter, in order to simplify the system and reduce its cost. The DC compressor speed can be adjusted according to the radiation intensity for an optimum match between PV output and the efficiency of refrigeration. During the daytime, the PCM is charged for cold storage by refrigeration; when solar radiation is weak or during the night, the PCM releases cooling to maintain the required cabinet temperature. A transient mathematical model is built for the whole system including PV module, DC compressor refrigeration system, fridge cabinet and PCM packs. The model is coded and solved in MATLAB while CFD method is used to produce some additional information. The simulations are conducted to evaluate the effect of solar radiation intensity, thermostat setting and the number of PCM packs on the fridge refrigeration performance. Moreover, the study aims to investigate and present benefits of incorporating PCM with a direct PV powered DC compressor fridge in weak/off-grid setting areas. When the fridge cabinet temperature varies between 4°C and -2°C, the average COP of the fridge refrigeration system was found 1.7 for high solar radiation day due to the high rotation speed of the compressor, but for low solar radiation day, the average COP was calculated as 1.95. The analysis also shows that a variable speed DC compressor can keep the foods in the desired temperature range for two days of power outage by using 1 m² PV module and 3.6 kg of thin PCM packs.

Keywords: DC compressor; Domestic fridge; Photovoltaics; PCM; Transient performance

1. Introduction

Electricity is the most important energy source for residential populations to maintain comfort and health in everyday life. However, electricity is still not accessible for about 18% of the world's population (Zubi et al. 2016). 590 million people did not have access to electricity in Sub Saharan Africa (SSA) and 240 million in India in 2016. Although the number of people decreased for India from 2000 to 2016, the population who cannot access electricity is increasing in SSA (International Energy Agency IEA 2019). As a result of this, food spoilage is a significant problem facing Africa/developing countries. A lack of effective ways to keep fruits and vegetables cool in hot climates is usually the reason for their loss. Cities in many SSA countries face the combined problems of rising temperatures and inadequate power supply. They do not have access to reliable electricity, if at all, and consequently do not have proper refrigeration/air conditioning systems

since existing technologies require higher quality grid electricity.

Therefore, developing sustainable and affordable refrigeration systems for food preservation requires urgent attention. To avoid grid problems and off-grid issues in rural areas, use of solar energy for cooling is an effective way which comes with many advantages universally considering environmental issues (Desideri, Proietti, and Sdringola 2009). Solar powered refrigeration can be categorised as PV driven and thermal driven systems (Su et al. 2020) and PV driven systems have advantages over thermal systems in space-effectiveness, cost and energy-effectiveness (Alrwashdeh and Ammari 2019; Sajid and Bicer 2021). PV technology requires very low maintenance and repair expenses, which make this technology operationally one of the most low-cost options (Sharma 2011; Kumar and Kumar 2017).

PV powered refrigeration systems have been investigated considering performance on different factors, such as PV voltage, compressor type, and controller methodologies. Daffallah et al. (Daffallah 2018) experimentally studied a PV powered DC refrigerator to present effects of ambient temperature, thermostat setting and

Department of Architecture and Built Environment, Faculty of Engineering, University of Nottingham, UK

Corresponding authors: Cagri Kutlu (cagri.kutlu2@nottingham.ac.uk); Saffa Riffat (saffa.riffat@nottingham.ac.uk)

operating voltage. They reported that the operation time and energy consumption of the compressor is higher in 24 V PV collectors compare to 12 V input when using the same refrigerator. As fixed speed compressors have been designed and well adapted for grid connected systems, commercial domestic refrigeration systems use fixed speed compressors to operate, however, their operation is affected in places in weak grid setting areas as voltage fluctuations cannot provide a smooth operation. Moreover, in order to connect with PV collectors, the system requires an inverter and battery as PVs generate DC current and solar radiation changes by time so, energy needs to be stored to start the compressor normally. Results of the additional components and their conversion efficiencies, PV connected AC compressor refrigeration systems have energy losses before refrigeration. In order to prove this, Opoku et al. (Opoku et al. 2016) conducted comparison experiments using a DC compressor and a AC compressor as different cases in PV driven refrigeration. In their test, the DC refrigeration system didn't have inverter, but batteries were adapted for both units. They presented that the DC refrigeration system is associated with less energy consumption and cost effectiveness. Parallel to this study, Sabry et al. (Sabry and Ker 2020) studied on the electricity consumption trend of an inverter-driven variable speed controller refrigerator. They investigated different component connections as battery-inverter-load, battery-load and grid-load of the DC refrigerator and finally AC refrigerator. Results show that battery-load consumes less daily power than traditional battery-inverter-load systems. Salilih et al. (Salilih and Birhane 2019) modelled PV refrigeration unit with variable speed DC compressor. They found that low rotation speeds yield higher COP value. Considering all literature findings, recently published paper by Su et al. (Su et al. 2020) proposed a PV powered variable speed DC refrigerator which directly connected to PV cells. They compared fixed speed and variable speed modes and found that variable speed mode increases cooling capacity and PV utilization.

Given references show performance improvement potentials and system configuration selections of PV powered refrigeration systems. However, without a backup battery, direct PV driven DC compressor refrigeration systems cannot provide cooling during night as solar energy is not available. Therefore, cold storage unit needs to be used in the cabinets to maintain the temperature in a desired range in order to maintain foods. Use of phase change material (PCM) in the fridges has been proposed by many researchers. Moreover, application of PCM in refrigerators has been highlighted as it improves cooling performance.

PCMs are incorporated into fridges on the condenser, on the evaporator, or inside the cabinet (Du et al. 2018) to obtain various benefits such as cold storage and more homogeneous temperature distribution in the fridge cabinet. As a cold storage, the PCMs have been used as a cold storage material in the fridges to keep fridge cold during power outage periods. Oro et al. (Oró et al. 2012) experimentally tested a freezer's low-temperature

capacity in case of a power failure by employing PCMs in the cabinet. They showed that temperature remains lower when PCMs are placed compared to case of without PCMs. Yilmaz et al. (Yilmaz, Mancuhan, and Yilmaz 2020) studied to see the influence of PCM locations in the cabinet and found that placement on the shelves keeps cabinet temperature more homogeneous and results in energy saving. Karthikeyan et al. (Karthikeyan et al. 2020) tested different PCM arrangements in the fridge and presented that using PCM can reduce temperature fluctuations and helps to preserve food quality. Moreover, other benefits of the use of PCMs in the refrigerators can be stated (Omara and Mohammedali 2020). For example, they improve heat transfer rates and reduces condensation temperature when used on the condenser side (Sonnenrein et al. 2015), and they increase the COP of the refrigeration units by reducing the pressure ratio of the evaporation and condensation (Elarem et al. 2017). Bahloul et al. (El-Bahloul, Ali, and Ookawara 2015) conducted an experiment to investigate the performance of the solar PV refrigerator. Their test was based on measurements for 23 days and the results showed that for setting temperature of 0°C, average COP value was found 1.22. Geete et al. (Geete, Singh, and Somani 2018) carried out a test by using PCMs in evaporator, COP improvement achieved up to 20%. Several papers can be found in the literature and all of them support the idea of PCM employment is a promising method to improve performance and other parameters in refrigeration applications. However, there is a lack of studies about the employment of PCMs and their effects on the fridge performance by using the transient modelling of direct PV driven variable speed DC compressor refrigerators.

In this study, a simplified mathematical model is presented to simulate the transient performance of a direct PV powered variable speed DC fridge incorporated with thin PCM packs. In order to maintain the desired temperature range in the fridge cabinet, different numbers of PCM packs and thermostat settings are tested in the simulations under chosen weather conditions with relatively low or high solar radiation. Particularly, CFD modelling is also employed to study the temperature distribution inside the fridge cabinet for different configurations of PCM packs. The findings of this study can provide some new useful information in development of direct PV powered variable speed DC fridge technology.

2. Material and methodology

As this study aims to sustain a cold temperature for a fridge, modelling on fridge cabinet includes PCM modelling to enhance cold storage performance. The importance of cold storage potential can be seen from **Figure 1**. The figure shows power outage frequency per month and average power outage duration for various countries (World Bank 2019). It can be seen from the figure that even the areas where electricity supply is normally possible, would need solar powered and PCM enhanced fridge to prevent foods spoiling. As the system proposes to use PV to run variable speed DC compressor, the proposed system can be used

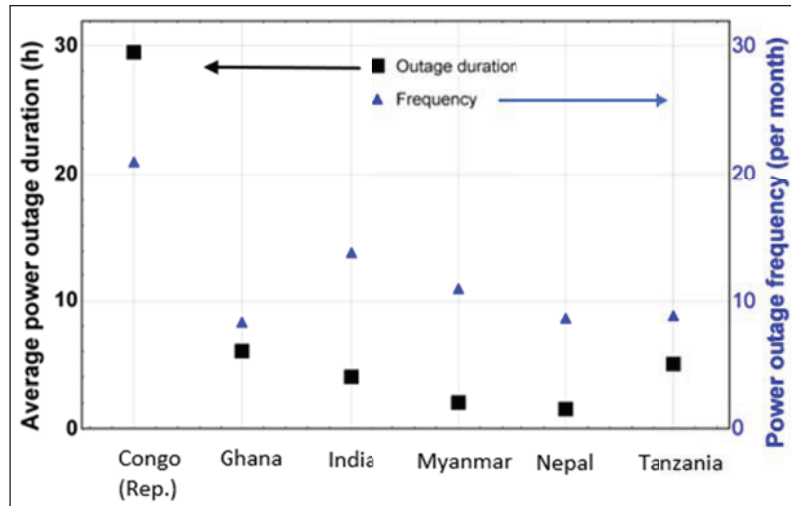


Figure 1: Weak grid electricity supply conditions for some developing countries.

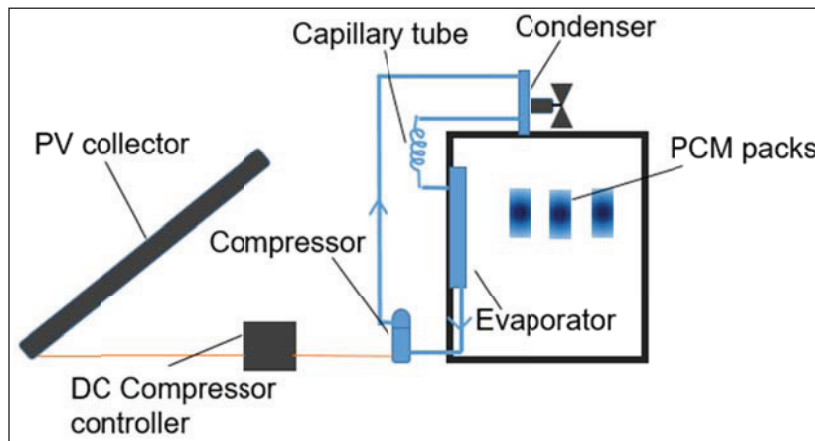


Figure 2: Schematic view of the system.

in urban areas. It is shown that in the event of an 8-hour power outage, a cold temperature should be provided by PCM cold storage units. We can assume that daytime electricity cuts can be supplied by solar PV, thus, 8-hour cold storage is the target. In order to show improvement, a conventional fridge and a PCM enhanced fridge are modelled and simulation results are presented. For cabinet air side modelling, CFD analysis is used to determine heat transfer coefficient and to validate PCM melting/freezing process in overall model.

3. Modelling of the system

The system has three sub-models namely, PV collector, refrigeration cycle and fridge cabinet. Figure 2 shows the components. PV collector generates DC current to run compressor. DC compressor controller adjusts compressor speed according to solar irradiance and refrigeration unit cools the cabinet with variable cooling loads. PCM packages are placed inside the fridge cabinet to heat exchange with air during the daytime.

3.1. PV model

Neglecting the losses in the controller, PV output power is equal to compressor input power. Maximum power point tracking (MPPT) method is applied on the simulations

because it is one of the mostly adopted method in the PV driven compressor studies. MPPT method in real applications, measured PV output voltage and current are used to find PV power output and compressor speed controller adjusts the speed. Later, PV power is measured again, and the controller adjusts according to power increment and decrement, This method has been applied in modelling work and validated by the experiment in the reference study (Gao et al. 2021). To make simplifications, this study calculates the PV output power by using one of the most popular methods for determining PV cell temperature called Normal Operating Cell Temperature (NOCT) method. Commonly preferred poly-Si type panels are chosen, and Table 1 shows the electrical characteristics of the modules. NOCT is given by the manufacturer and Eq. (1) can be used for calculating the cell temperature (Mattei et al. 2006).

$$T_{cell} = T_a + (NOCT - 20) \cdot \frac{G}{800} \quad (1)$$

Electrical efficiency of the PV is calculated by Eq. (2):

$$\eta_{PV} = \eta_r [1 - \beta_r \cdot (T_{cell} - T_{ref})] \quad (2)$$

is efficiency at the reference temperature.

Table 1: Specifications of used PV module (Santiago et al. 2018).

Specifications	
Model	Atersa A-214P
Type	Polycrystalline silicon
Module efficiency, η_r	12.64%
Power temperature coefficient, β	-0.0046/K
NOCT	47°C

3.2. Sub-model for refrigeration cycle

The refrigeration system has four components: compressor, condenser, capillary tube and evaporator. The following assumptions are considered for refrigeration simulation (Kutlu et al. 2019):

- The evaporation in the evaporator and condensation in the condenser are assumed to be constant pressure process.
- The expansion of the refrigerant in the capillary tube is assumed to be adiabatic.
- Subcooling in the condenser is assumed 3K but superheating in the evaporator will be calculated in modelling.

3.2.1. Model of compressor

In the system a miniature compressor is used because the proposed compressor can operate with 12V and 24V sources which makes it suitable for PV applications. Its displacement volume is 1.9 cm³ with rated refrigerating capacity of 245 W and rated input power is 85 W.

The compressor model provides not only the power for compression but also the working fluid mass flow rate. In order to derive mass flow rate \dot{m} Eq. (3) is given:

$$\dot{m}_r = \eta_v \cdot V_{sw} \cdot N \cdot \rho_1 \tag{3}$$

V_{sw} indicates swept volume of the compressor, N is compressor speed, ρ_1 is density of the compressor inlet and η_v is volumetric efficiency. For volumetric efficiency, an

empirical equation is adapted from Borges et al. (Borges et al. 2010).

$$\eta_v = 0.576 - 0.0162 \cdot (P_{con}/P_{ev}) \tag{4}$$

Regarding the isentropic efficiency of the compressor, Marques et al. (Marques et al. 2014) analysed different size of compressors' isentropic efficiency variations with different evaporating temperatures. They used compressor unit selection tool program RS+3 developed by Danfoss to predict performance data using 35°C condensing, 25°C ambient, 1K superheating and 15°C compressor suction temperature. The results of the isentropic efficiency variations are shown in **Figure 3**. As pressure difference in this study is expected to be between 4 and 6.5, isentropic efficiency will variate between 0.45 and 0.4. Thus, the isentropic efficiency is taken as 0.45.

3.2.2. Model of condenser and evaporator

For modelling of condenser, dimensioning of the heat exchanger was not calculated in this model as condenser has a fan and it can be assumed that condensing temperature is 10 K higher than the room temperature at the beginning (Hundy 2016). Later, system control method will be explained, and temperature will be adjusted easily if condenser temperature needs to be increased.

The refrigerant flows in the evaporator via pipes. As superheating heat transfer is small compared to evaporation, the temperature of the refrigerant will remain constant in the heat exchanger as phase change occurs.

The energy balance equation of the evaporator's wall is given in Eq. (5):

$$M_{ev} \cdot c_{ev} \cdot \frac{\partial T_{ev}}{\partial t} = A_p \cdot h_{ref,p} \cdot (T_r - T_{ev}) + A_{ev} \cdot h_{air} \cdot (T_{air} - T_{ev}) \tag{5}$$

As refrigerant boils in the pipe, fluid is in two-phase state. For boiling in the evaporator, the Kenning-Cooper correlation in Eq. (6) can be used revised by Sun and Mishima (Sun and Mishima 2009).

$$h_{ref,p} = [1 + 1.8X^{-0.87}] \cdot 0.023 Re_p^{0.8} Pr_p^{0.48} (k/d) \tag{6}$$

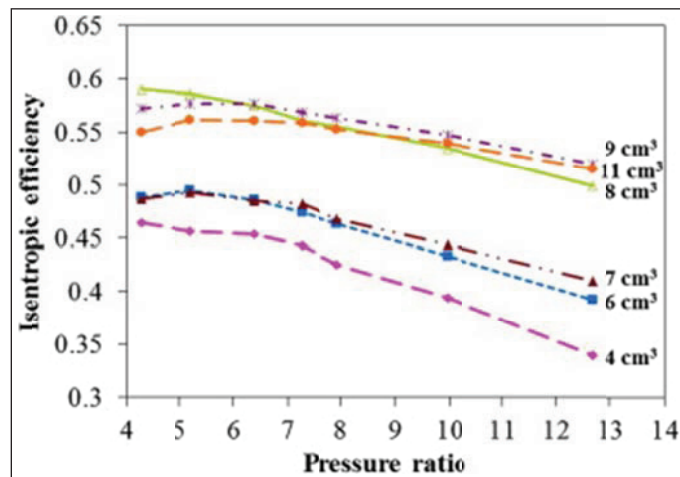


Figure 3: Variation of isentropic efficiency with pressure ratio for different capacity of compressors (Marques et al. 2014).

where capital "X" is the Martinelli factor which is calculated from vapour quality 'x':

$$X = \left(\frac{1-x}{x} \right)^{0.9} \left(\frac{\rho_v}{\rho_l} \right)^{0.5} \left(\frac{\mu_l}{\mu_v} \right)^{0.1} \quad (7)$$

3.2.3. Model for capillary

Capillary element reduces pressure and temperature of the refrigerant but also determines flow rate. Empirical equation created by Jung et al. (Jung, Park, and Park 1999) is used:

$$\dot{m}_{cap} = C_1 \cdot D_{cap}^{C_2} \cdot L_{cap}^{C_3} \cdot T_{con}^{C_4} \cdot 10^{C_5 T_{subcool}} \quad (8)$$

Where, C are empirical numbers which can be find in the reference paper, D and L are diameter and length of the capillary, respectively.

3.3. Transient model for the fridge cabinet

The cabinet sub-model provides calculation of the temperatures in the refrigerated compartments over time. Air temperature variation is calculated for each time step considering heat gain from room, cooling load from the evaporator, heat transfers from thermal mass in the fridge and PCM. Although it is known that air velocity in the fridge varies and temperature stratification occurs in the fridge cabinet, this study uses a simplified approach which assumes uniform air temperature in the fridge (Azzouz, Leducq, and Gobin 2009) in order to use solar powered refrigeration system performance. Control volume of the air is exposed to heat gain from the room, heat extraction by the evaporator and heat transfer with PCM packs. A schematic is given to show exposed heat transfers to the control volume of the air in **Figure 4**. Direction of the heat flow is determined by the temperatures of the components at specified time.

Additionally, to refer some food in the fridge, modelling also includes thermal mass in the cabinet.

$$\dot{Q}_{tm} = A_{tm} \cdot h_{tm-air} \cdot (T_{tm} - T_{air}) \quad (9)$$

Similarly, air side PCM heat transfer equation can be written. Heat transfer rate from room to the cabinet is calculated by Eq. (10). $U_{overall}$ comprises outside wall and inside

wall heat transfer coefficients and wall conduction coefficient which includes insulations.

$$\dot{Q}_{gain} = A_{cabinet} \cdot U_{overall} \cdot (T_{room} - T_{air}) \quad (10)$$

By using given equations, energy balance of the air in the fridge cabinet is given in Eq. (11).

$$M_{air} \cdot c_{air} \cdot \frac{\partial T_{air}}{\partial t} = A_{ev} \cdot h_{air} \cdot (T_{ev} - T_{air}) + \dot{Q}_{PCM} + \dot{Q}_{tm} + \dot{Q}_{gain} \quad (11)$$

As fridge cabinet is an enclosure, heat balance will give us temperature variations of the components. \dot{Q}_{ev} , \dot{Q}_{PCM} , \dot{Q}_{tm} and \dot{Q}_{gain} indicate air side heat transfer rates from evaporator plate, PCM packs, thermal mass, heat gain and heat transfer rates.

Heat transfer coefficients in the cabinet can be calculated however, as the air is assumed as uniform, average heat transfer coefficient need to be determined. In this study, CFD tool will be used to find average heat transfer coefficient inside the cabinet.

3.3.1. Modelling of the PCM pack melting and solidification by CFD tool

In order to increase heat transfer surface area, thin PCM packs are chosen to use for cold storage units, **Figure 5** shows used PCM pack and its dimensions. In order to solve numerical simulations, 275170 elements were created for

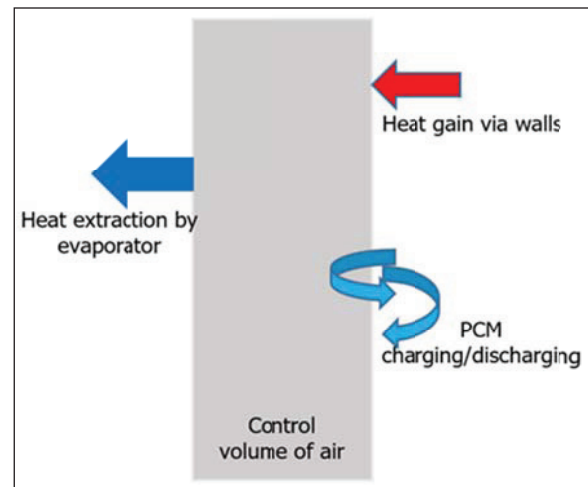


Figure 4: Energy flows inside the fridge cabinet.

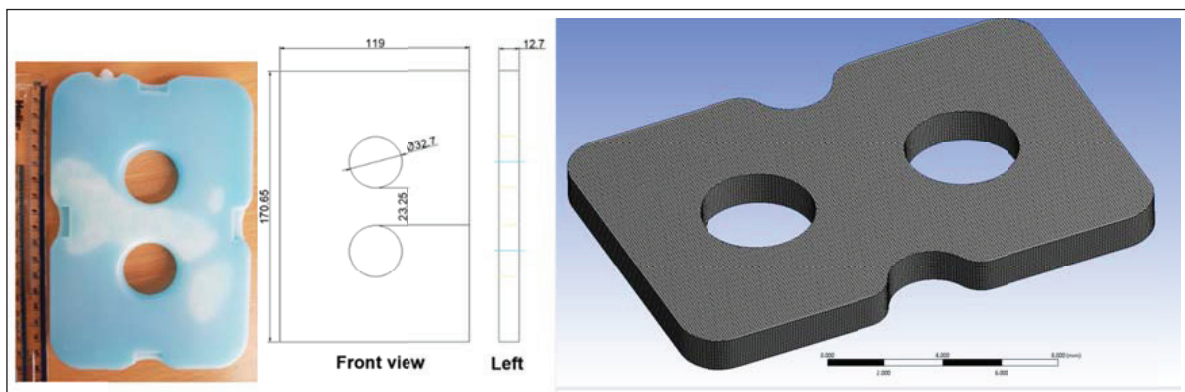


Figure 5: PCM pack dimensions and mesh profile.

Table 2: Thermophysical properties of A4 (Phase Change Material Products, 2020).

Specific heat	2.18 kJ/kgK	Latent heat capacity	235 kJ/kg
Density	766 kg/m ³	Thermal conductivity	0.21 W/mK

packs by software ANSYS fluent. Organic PCM A4 is used which has melting temperature of 4°C. Used PCM properties are summarised in **Table 2**.

Regarding to modelling, there are three well-known models available in the literature to solve melting and solidification problems through CFD analysis: equivalent heat capacity method, enthalpy method and temperature transforming model (Lamberg, Lehtiniemi, and Henell 2004; Ghahramani Zarajabad and Ahmadi 2018).

The enthalpy-porosity method is adapted for modelling the melting process of PCM unit. The PCM properties are assumed as constant and given in **Table 2**. The density of PCM is modelled with Boussinesq approximation to neglect volume expansion in the PCM via natural convection (Mahdi et al. 2020). The governing equations are given below:

$$\nabla^2 \vec{V} = 0 \quad (12)$$

$$\rho \frac{\partial \vec{V}}{\partial t} + \rho (\vec{V} \nabla) \vec{V} = -\nabla P + \mu \nabla^2 \vec{V} + \rho \beta \bar{g} (T - T_0) + \bar{S} \quad (13)$$

Conservation of energy:

$$\frac{\partial}{\partial t} (\rho H_e) + \nabla \cdot (\rho \vec{V} H_e) = \nabla \cdot (k \nabla T) \quad (14)$$

Enthalpy (H_e) is the total heat content of the PCM which is sum of sensible (h_e) and latent heat (ΔH_e). Eq. (15) is given for enthalpy.

$$H_e = h_e + (\Delta H_e) \quad (15)$$

Where, sensible heat is:

$$h_e = h_{e_o} + \int_{T_o}^T c_p dT \quad (16)$$

The latent heat during the phase change is given in Eq.(17).

$$\Delta H_e = \lambda \cdot Lat \quad (17)$$

where Lat is the latent heat of fusion of the PCM, and λ is the liquid fraction,

$$\lambda = \begin{cases} = 0 & T < T_{solid} \\ = \frac{T - T_{solid}}{T_{liquid} - T_{solid}} & T_{solid} < T < T_{liquid} \\ = 1 & T > T_{solid} \end{cases} \quad (18)$$

In order to solve momentum equations and pressure equations, second-order upwind scheme and PRESTO scheme are used, respectively. The under-relaxation factors for the velocity components, liquid fraction, pressure, and energy are set at 0.7, 0.9, 0.3 and 1, respectively (Mahdi et al. 2020). The convergence criteria for the residuals of the continuity equation, momentum equation and energy equation are 10^{-5} , 10^{-5} and 10^{-9} , respectively (Mahdi et al. 2020).

3.3.2. Modelling of the PCM pack melting and solidification in overall MATLAB model

When PCM is placed inside the fridge, both sensible and latent heats constitute the total heat capacity of the fridge and heat transfer from air to PCM, or vice versa, is taken into consideration (Kutlu et al. 2020). To simulate heat transfer process, some assumptions are considered for modelling in MATLAB.

PCM energy balance equation is generalized by Manfrida et al. (Manfrida, Secchi, and Stańczyk 2016)

$$V_{PCM} \cdot \rho_{PCM} \cdot Lat_{PCM} \cdot \frac{\partial \lambda}{\partial t} - V_{PCM} \cdot \rho_{PCM} \cdot c_{PCM} \cdot \frac{\partial T}{\partial t} = h_{air-PCM} \cdot A_{air-PCM} \cdot (T_{air} - T_{PCM}) \quad (19)$$

λ is PCM liquid fraction, $h_{air-PCM}$ is heat transfer coefficient between the PCM pack and cabinet cold air. Where the PCM packs were divided into several equal layers, energy balance equation was applied to each layer. Given assumptions were adopted to simplify the mathematical model (Marques et al. 2014):

- Thermophysical properties of the PCM were assumed as constant during the simulation (thermal conductivity, density, latent heat).
- Only conduction heat transfer was considered between PCM layers and inside the PCM (Convection heat transfer was neglected during melting).
- There is no supercooling in the PCMs.
- The PCM container walls were assumed to be very thin and didn't included heat transfer equations.

4. Results and discussion

4.1 CFD analysis for heat transfer coefficient

The study also aims to find out the impact of the amount of PCM placed in the cabinet on performance of a fridge operating in standard conditions. Before conducting an overall performance simulation, a numerical model was built to predict the total heat transfer and storage time during charging and discharging of PCM packs by CFD analysis. After several simulations to find exact mass requirement for desired time and temperature, 18 packs were determined for analysis.

By using standard under counter fridge dimensions and insulation properties, the system set up was prepared. The PCM packs are placed in the fridge and air temperature is at uniform 0°C and PCM temperature is assumed as the same with the air temperature initially. 18 PCM packs (3.6 kg) are located with 20 cm distance between each group from top to bottom and simulation is conducted for three hours of compressor off period. **Figure**

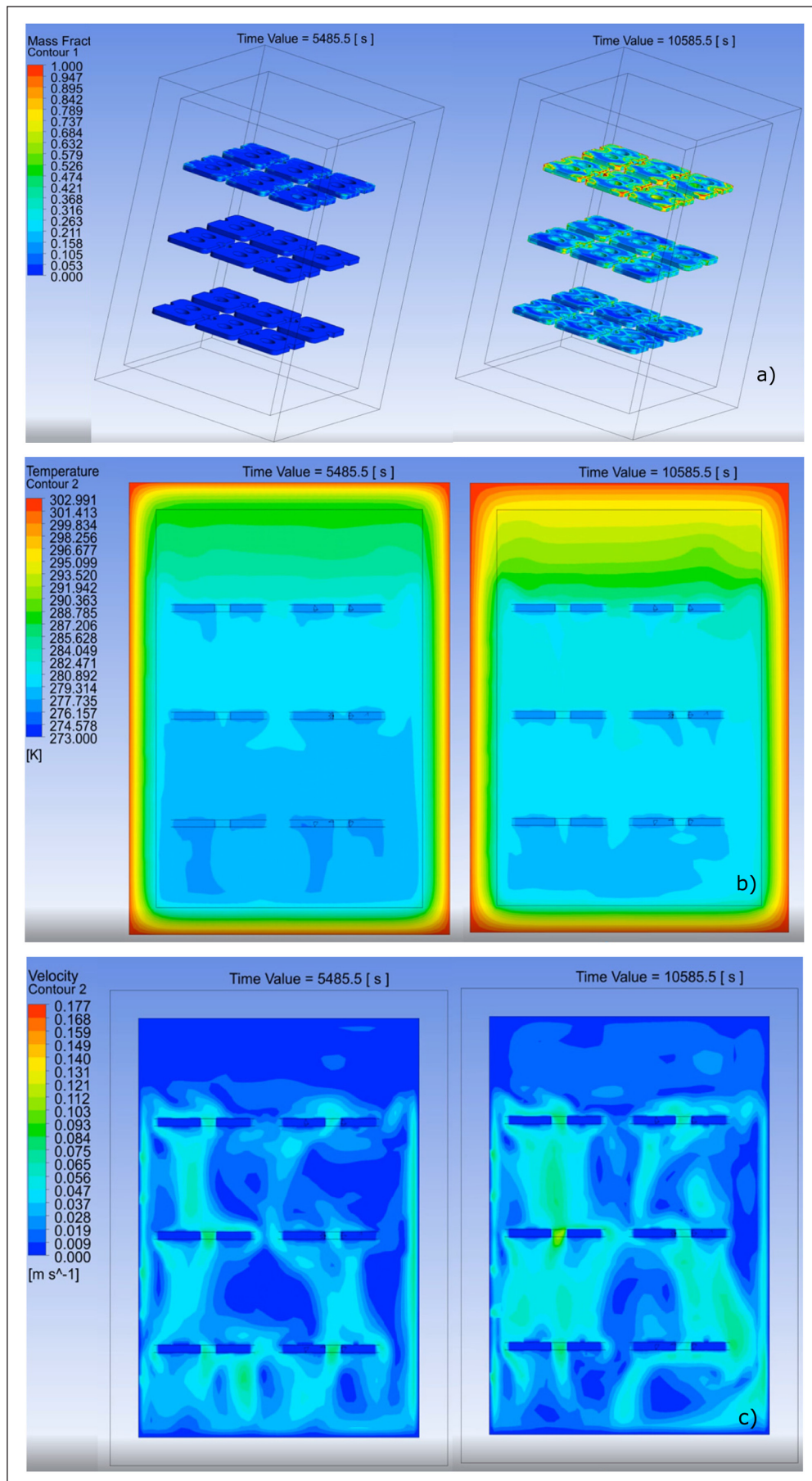


Figure 6: Mass fraction, temperature and velocity contour variation in the 18-PCM pack fridge (room temperature: 30°C) (91–176 minutes).

6a shows liquid-fraction of the PCMs by time. According to the figure, upper level PCMs melt faster because of high temperature air is collected in top. At the end of the simulation, volume average air temperature reaches 10°C. However, volume average temperature means some parts of the fridge can be higher and some parts can be lower temperature. In order to see it, **Figure 6b** shows temperature gradient in the fridge. As expected, upper parts are higher temperature than the rest. After 3-hour, lower part of the fridge is still at 6°C this is promising for keeping the temperature at desired level. **Figure 6c** shows velocity contour variation in the fridge. As expected, upper level is more stable but lower levels have significant air movements especially between PCM packs. Air near to walls moves up because of lower density, when hot air touches to the PCM goes down. It is good to observe that PCM packs helps to air movement with the holes on the middle. These holes allow cooled air to go down and highest air flow velocity occurs. This simulation shows the importance of the design of the internal fridge. The shape of the PCM pack and its location has significant influence of the temperature gradient in the fridge. Pavithran et al.

(Pavithran, Sharma, and Shukla 2020) presented in their study that amount and the area coverage of PCM has an influence on temperature stabilization inside the fridge. They suggested that area coverage should be more than 10% of the total area of the inside fridge.

The main aim of the CFD analysis is to determine heat transfer coefficient between cold air and the items inside the cabinet. Since the modelling is based on average air temperature approach, heat transfer coefficient was calculated considering average PCM surface temperature and average air temperature. **Figure 7** shows variation of the heat transfer coefficient based on calculation. It increases by time which refers temperature difference increment between average air temperature and PCM surface temperature.

4.2 Method of solution

The transient model of the overall system (includes refrigeration cycle, PV module, fridge cabinet and PCMs) is developed in MATLAB environment and solved by iteration. Design parameters and units are given in **Table 3**. The thermophysical properties of the refrigerant were taken from REFPROP.

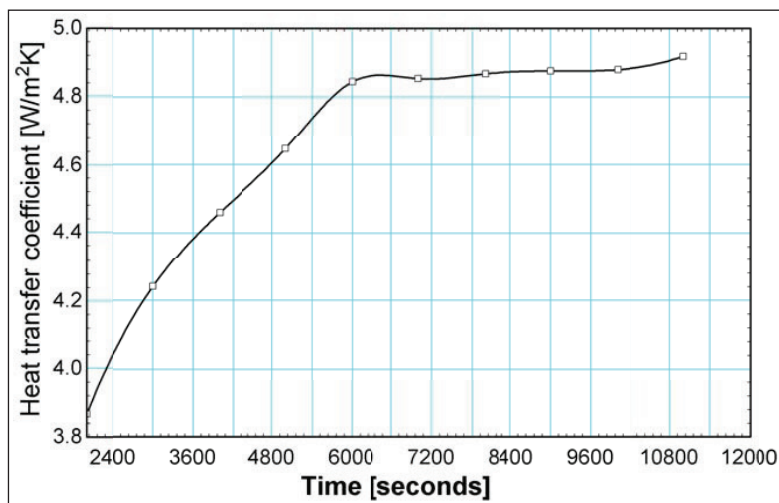


Figure 7: Variation of average heat transfer coefficient on PCM packs.

Table 3: Design parameters of the refrigerator system.

Component	Parameter	Value
PV collector	Area	1 m ²
Cabinet	Outer dimensions	84 cm × 55 cm × 60 cm
	Wall thickness	5 cm
Compressor	Displacement	1.9 cm ³
	Isentropic efficiency	0.45
Condenser*	Subcooling	3 K
Capillary tube	Inner diameter	0.65 mm
	Length	2.9 m
Evaporator	Outside diameter of pipe	8 mm
	Length	10 m
Refrigerant	R134a	

* Condenser is a fin and tube type, as there is a 12V fan adapted to operation, constant subcooling is assumed.

The solution flow chart of the simulation is shown in **Figure 8** and the solution steps are given in detail as follows:

- Before starting the simulation, a pre-analysis has been conducted to determine the heat transfer coefficient inside the fridge, based on findings of the CFD study. In the simulation, the design parameters of the components and initial conditions are written. These are component dimensions and properties, room temperature, initial temperatures of the components. As an initial condition, condensing temperature and evaporation temperature are assumed as 10 K higher from the room temperature and 10 K lower from the fridge temperature, respectively.
- PV electricity output is calculated considering weather conditions by Eqs. (1–2), this output will be the compressor consumption rate. Referring to the Eqs. (3–4), volumetric efficiency rotation speed and of course mass flow rate is found based on initial conditions. In the next time steps, temperatures will be taken at the end of previous time step values.
- By taking 3K subcooling, the capillary model is solved. If the flow rate in the capillary is different from calculated in the compressor, condenser pressure is adjusted, higher condensing pressure yields a higher flow rate in the capillary. The error criteria for adjustment is chosen as 10^{-2} .
- Solving the evaporator model, heat transfer rates can be found between refrigerant and evaporator tube, and also fridge air and evaporator tube. If the enthalpy of the refrigerant at the evaporator outlet is different from the compressor inlet in the compressor model, evaporating temperature and pressure are adjusted in the compressor model all calculations are repeated with these new temperatures.

- During finding the evaporator tube temperature, heat transfer between air and evaporator pipe is already considered. However, air temperature in the cabinet is also changed by heat gain via walls, heat transfer between PCMs, and thermal masses (water bottles).
- Each element has its own energy balance equations and the last temperatures are found at the end of the time step. The same procedure is followed for next time.

4.3. Validation of the model

Before the study was used for several cases, a validation with a refrigerator had been performed. This part focuses on validity of the simplified air modelling in the fridge. An experimental setup was prepared by using a commercial refrigerator shown in **Figure 9**. Compressor off mode is simulated and tested. Before the test, the compressor was run and air temperature was reached to -4°C . Then, five water bottles were placed in the cabinet at 6°C . In the figure, average of the measured air temperatures (top, middle and bottom) was used but more measurement is required to match with the uniform air approach as temperature is not uniform in the cabinet in real case. Since the heat gain occurs via the walls of the fridge and the temperature of the air near the walls increases, an air movement is obtained with a direction to the top section as the high-temperature air density is lower than cold air. Referring to the conducted CFD study in **Figure 6**, slightly higher temperature air is accumulated in the top section of the cabinet. However, this temperature difference in the CFD study happened after a 3-hours period. In the tested cabinet, the temperature difference between measured and calculated reaches a maximum of 1°C however, the top section temperature would be higher. However, the calculated water temperature was found close to the measured water temperature as water bottles are placed on two shelves to obtain average.

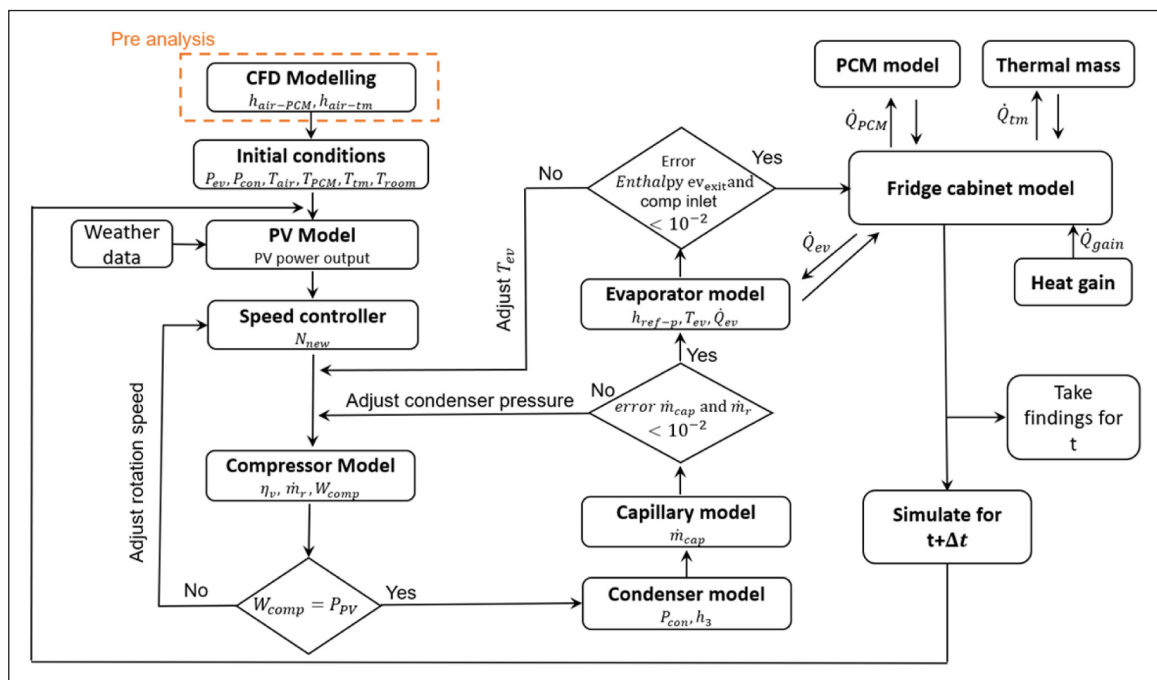


Figure 8: Flow chart of the simulation.

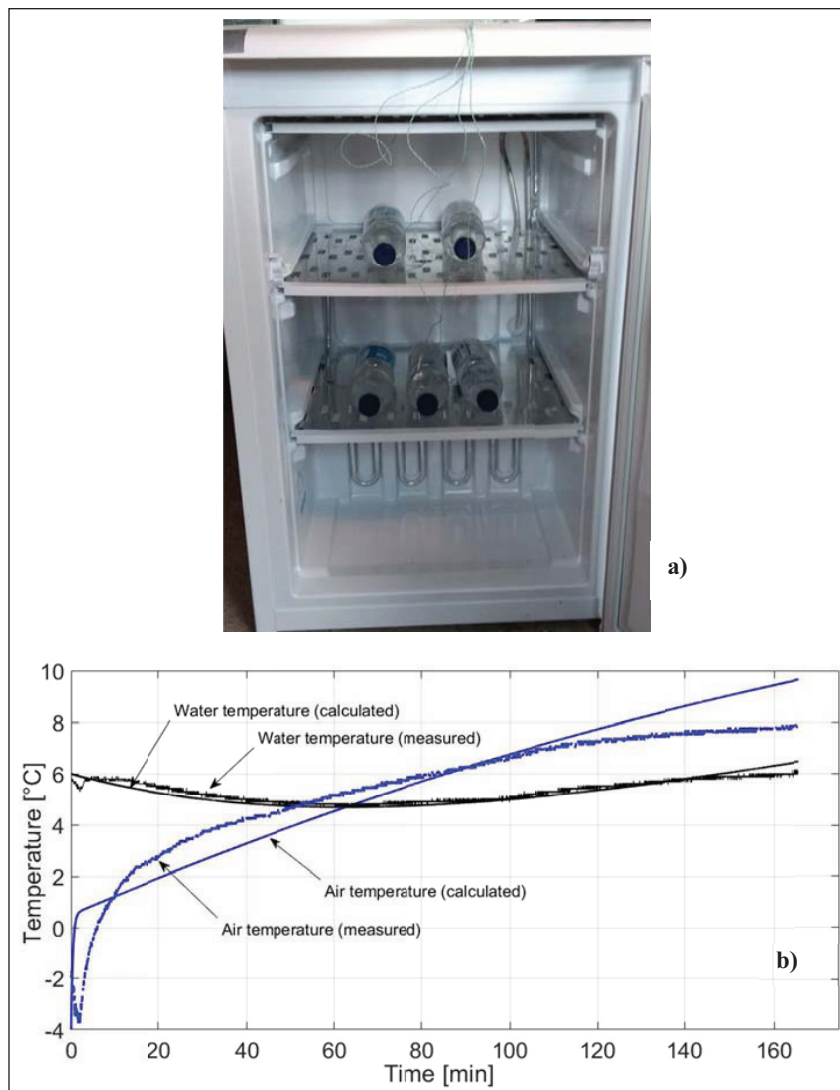


Figure 9: Tested fridge and average temperatures of water and air inside (experimental and simulation).

4.4. Simulations

Transient simulations are conducted to evaluate the effect of temperature setting points and solar radiation intensity on the temperature of the fridge cabinet and the fridge refrigeration performance metrics namely compressor consumption, on-off time, and rotation speed. As a second evaluation, the effect of the number of PCM packs is investigated.

Given system settings are applied on simulations:

- A thermostat in the fridge is modelled to keep the cabinet temperature between 4°C and -2°C. This means when the temperature reaches 4°C, the compressor starts to operate and stops when the temperature reduces to -2°C.
- The compressor speed is limited between 2000 RPM and 4500 RPM.

4.4.1. Solar data

The proposed system has no battery unit but has a variable speed DC compressor. To show the system's flexible operation ability, high and low solar radiation data are used in the simulations. The high solar radiation data is

taken from Photovoltaic Geographical Information System website (PVGIS,2020) for average hourly solar data in April in Ghana. In order to study the influence of solar radiation, the typical solar data was multiplied by 0.6 and low solar radiation was obtained. **Figure 10** shows high solar radiation and low solar radiation profiles used in the simulations.

In order to show higher solar utilization of the variable speed compressor over constant speed one, a comparison is made to show working hours in a day under given two different solar radiation levels. **Figure 11** shows the working range of the compressors. Variable speed compressor can work around 1 hour more on high solar radiation day. In low solar radiation day, the time is increased because the variable speed can start to operate at 2000 RPM. These early start and late stop times have significant advantages in temperature levels and required PCM amounts in the cabinet.

4.4.2. Effects of thermostat setting point

In this subsection, the effect of thermostat setting temperatures is investigated. As it is known, setting point affects the power consumption directly and its selection should be related to the application and the contents in the

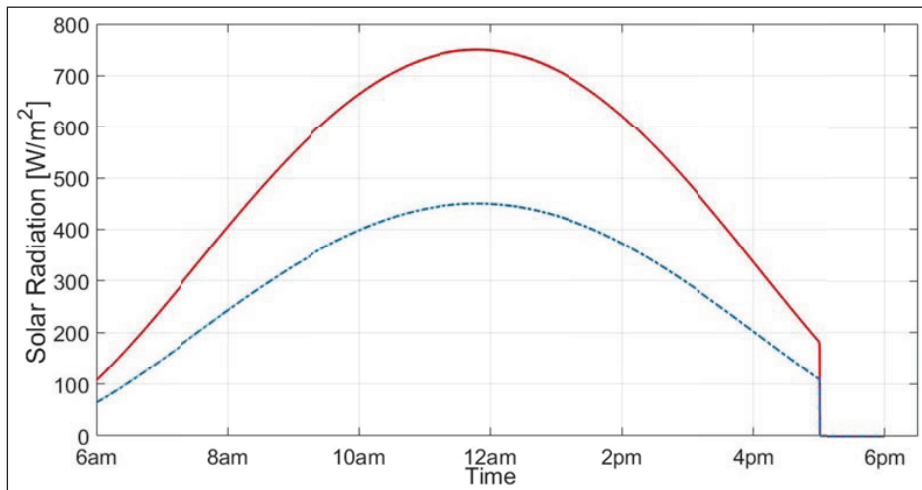


Figure 10: High solar radiation and relatively low solar radiation (dashed line) days.

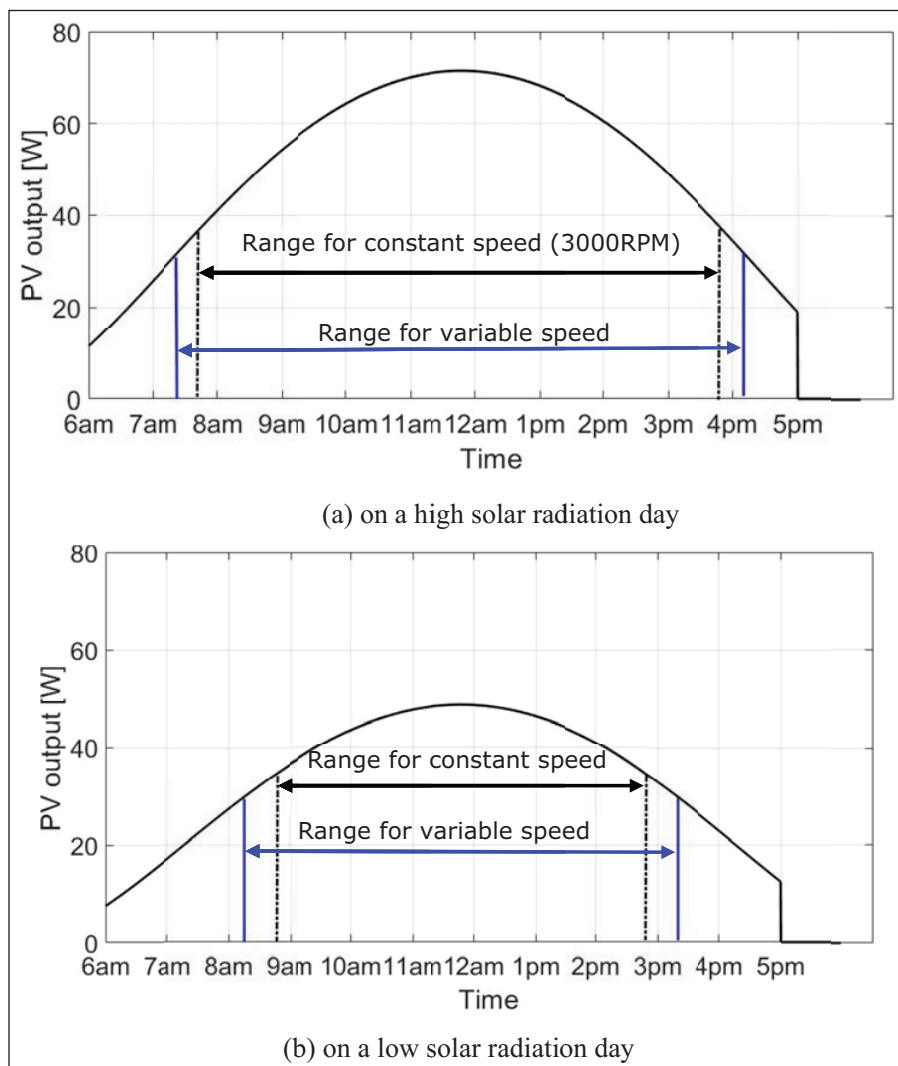


Figure 11: Range of working time for the variable speed and constant speed compressors, respectively.

fridge. Temperature settings of fresh food compartment of the refrigerators are given from 3°C to 5°C by manufacturers (Refrigerator, 2020). The thermostat setting temperature cannot assure to maintain this temperature since door opening and heat load from the room increases

temperature and during compressor-on times, the air temperature reduces. In order to see air temperatures in domestic refrigerators, a number of surveys and measurement studies have been taken. James et al. (James, Evans, and James 2008) presented a table by combining studies

around the world and stated that mean temperatures varied between 4.9°C to 7°C. Breen et al. (Breen et al. 2006) measured air temperatures in domestic refrigerators in the UK based study, their recorded temperatures varied from 1°C to 12°C but only 33% of the data were above 5°C. Therefore, three different settings are applied in this analysis, namely; 8°C to 0°C, 6°C to 0°C and 4°C to 0°C. Initial conditions and ambient conditions were kept the same in the analysis. The initial conditions of the simulations are given as: the PCMs are in the solid-state at 4°C, air is 11°C, room temperature is 25°C and high solar radiation data is used. **Figure 12a** shows temperature variations for three cases. As expected, compressor start-stop frequency is lower in 8-0 setting. In normal grid operation, this setting yields higher energy efficiency, however, solar-powered refrigeration units can operate as long as PV output is enough, and so, it is not necessary to consider energy efficiency. Moreover, states of the PCMs need to be considered. **Figure 12b** shows the average liquid fraction of the PCM packs in the fridge for the cases. 8-0 operation increases the liquid fraction even in the day time. The setting of 4-0 can keep PCMs in solid-state until evening, but in order to recharge the PCMs in order to use for the next day, the setting temperature should be lowered. Although the setting for practical applications is 8°C and 0°C, this

study aims to keep PCMs ready for evening periods as PCM melting temperature is 4°C. Therefore, the setting temperature for the cabinet is chosen at 4°C and -2°C.

4.4.3. Effect of solar intensity

By using high and low solar radiation levels, comparison simulations were carried out to investigate results on performance. In 12 hour-simulations, previously determined 18 PCM packs are placed in the cabinet at 4°C in solid-state, evaporator and 6 litres of water at 6°C have been used as initial conditions by using 4°C and -2°C setting temperatures. Comparison results are given in **Figure 13**. Firstly, compressor speeds are shown in **Figure 13a**. Since PV electricity generation is less in the low solar radiation day, compressor input power is lower which leads to the compressor's late starting time. In both cases, the compressor rotation speed is low at the beginning because the evaporator temperature is relatively high. Its temperature falls over time and compressor inlet density decreases. **Figure 13b** shows compressor consumption profiles of both cases during the day. Related to PV output power, consumption increases in the midday as solar radiation is higher. Also, compressor on-off times can be seen from the figure. On the low radiation day, the refrigerator cannot operate before 8 am, and after 3 pm periods as power

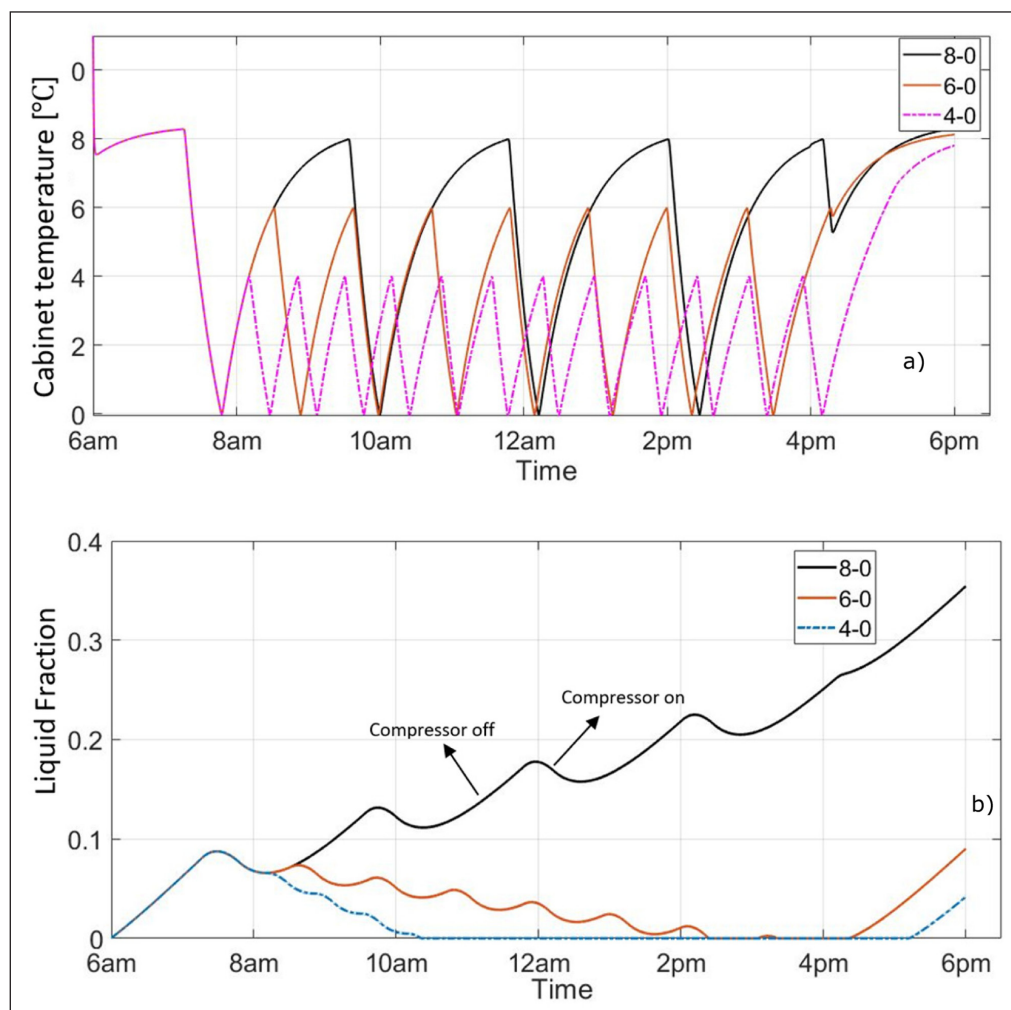


Figure 12: Temperature change in the cabinet (a), and average PCM liquid fraction (b) for different thermostat setting temperatures.

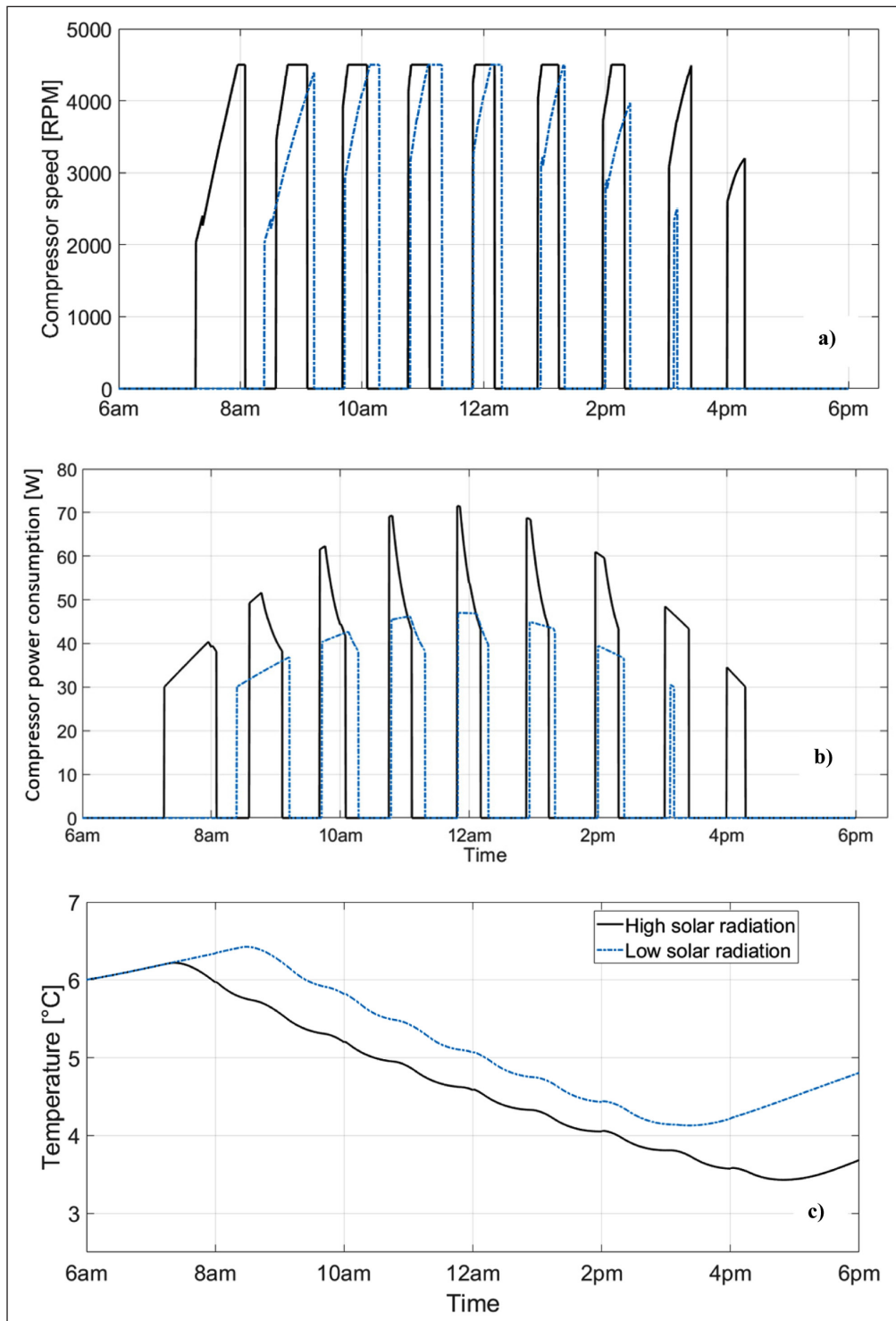


Figure 13: Comparison of (a) rotation speeds, (b) compressor consumptions, (c) water temperature variation.

generation from the PV is insufficient. Operation time for each compressor-on mode takes longer time on low radiation days, this is a result of a lower instant cooling load. Low cooling load is not desired, however, thermostat setting eliminates this effect because cooling time takes a longer period to balance it. When the compressor is off, the excess power can go to the grid. **Figure 13c** shows the temperature change of the water. Although the initial temperatures are the same, water temperature begins to decrease before 8 am as the aforementioned reasons in high radiation day. Late start of cooling operation causes

0.5°C lesser water temperature in low solar radiation day. However, at the end of the day, water temperature is higher than the beginning, thus, it needs to be analysed for the following days. Two days of simulations will be conducted in the following sections.

4.4.4. Effect of PCM mass

In this section, different amounts of PCM packs are simulated in the cabinet considering 4°C and -2°C setting temperatures and initial conditions. In order to observe the influence of the PCM amount, two-day simulation is

required to include the previous day's charging-discharging effects and to test the system under different weather conditions. The solar data given in **Figure 10** is used for two days of operation. It is assumed that high solar radiation level is used on the first day, low solar data is for the second day. All temperatures at the end of the first 24 hours are the initial temperatures for the second day.

Figure 14 gives the temperature variation of the water for two days for different cases. In the first case, 18 PCM packs have been used (3.6 kg) and the temperature of the water is kept in the desired range after the second day. In the second case, 16 PCM packs have been used (3.2 kg) and a similar trend is observed with the first case on the first day. However, the water temperature reaches higher during the first night and continues the following day. This trend is a result of smaller PCM surface area as PCM heat absorption remains relatively lower in Case 2. In case 3, 10 PCM packs (2 kg) have been used in the cabinet. 10 packs mean lesser PCM mass and heat transfer area which results in the worst performance. First cooling period (the first day from 8 am to 5 pm) water temperature in 18 packs case falls from 6.2°C to 3.4°C but for 10 packs case, it decreases from 6.35°C to 3.8°C. Although the solar radiation level is kept the same for both cases, water temperature is higher at the beginning of the cooling process for 10 packs case because of lower heat transfer area between the PCMs and cabinet air. In the second cooling period, water temperature falls from 6.7°C to 4°C.

4.4.5. Two days performance

By using the weather data from **Figure 10** and considering the same method of the previous section, two days performance data is given in this section. **Figure 15** shows performance metrics of the two days simulation when 18 packs are used. **Figure 15a** gives water and cabinet temperature variations. Since the first day of the simulation is based on initial conditions, second day will give better information on performance. On the second day, the com-

pressor starts only five times because of low solar radiation. These low number of cooling periods also affects PCM charging. As the result of insufficient recharging on the second day, stored latent heat in the PCM packs are consumed by the midnight.

Figure 15b shows condensation and evaporation temperature variation during the simulations. Since compressor rotational speed is related to solar intensity, the refrigerant mass flow rate increases in midday. The capillary model increases the condenser pressure to allow flow through the refrigerant inside the capillary. Similarly, second day condensation temperature is lower than the first day as second day has lower solar radiation. **Figure 15c** gives COP variation during the simulations. Although the cooling load is lower because of low solar radiation, average COP is higher in the second day because low solar radiation yields lower rotation speed of the compressor. Referring to **Figure 15b**, calculated condensation temperature is lower in second day compared to high solar radiation day. Moreover, lower cooling load decreases the evaporation temperature slowly. Relatively lower condensation and higher evaporation temperatures result better COP in low solar radiation day.

The average results obtained from the simulations can be summarized as given. The effect of the thermostat setting temperature on liquid fraction was simulated under high solar radiation day when 18 PCMs pack used. It was found that high-temperature setting increases the liquid fraction. Therefore, the setting temperature for the cabinet was chosen at 4°C and -2°C for the rest of the simulations. Different amounts of PCM packs were simulated in the cabinet and final water temperatures at the end of the simulation were found 13.7°C, 8.1°C and 7.8°C, for the cases of 10, 16 and 18 packs, respectively. The effect of the solar radiation on water temperature was simulated and water temperature at the end of the day was found 3.6°C for high solar radiation day and 4.8°C for low solar radiation day.

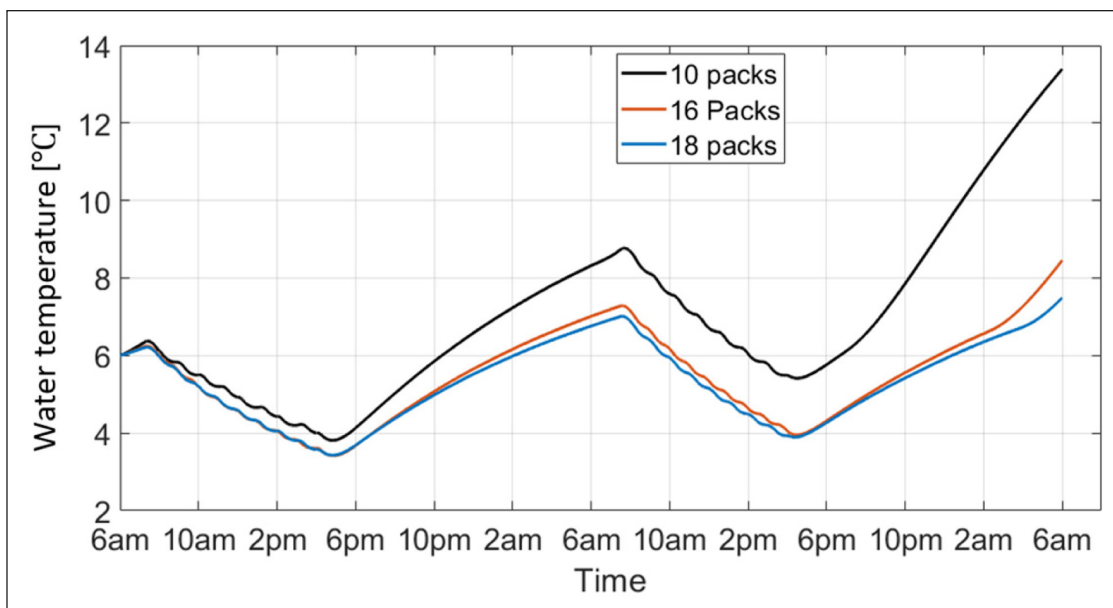


Figure 14: Effect of the number of PCM packs on water temperature.

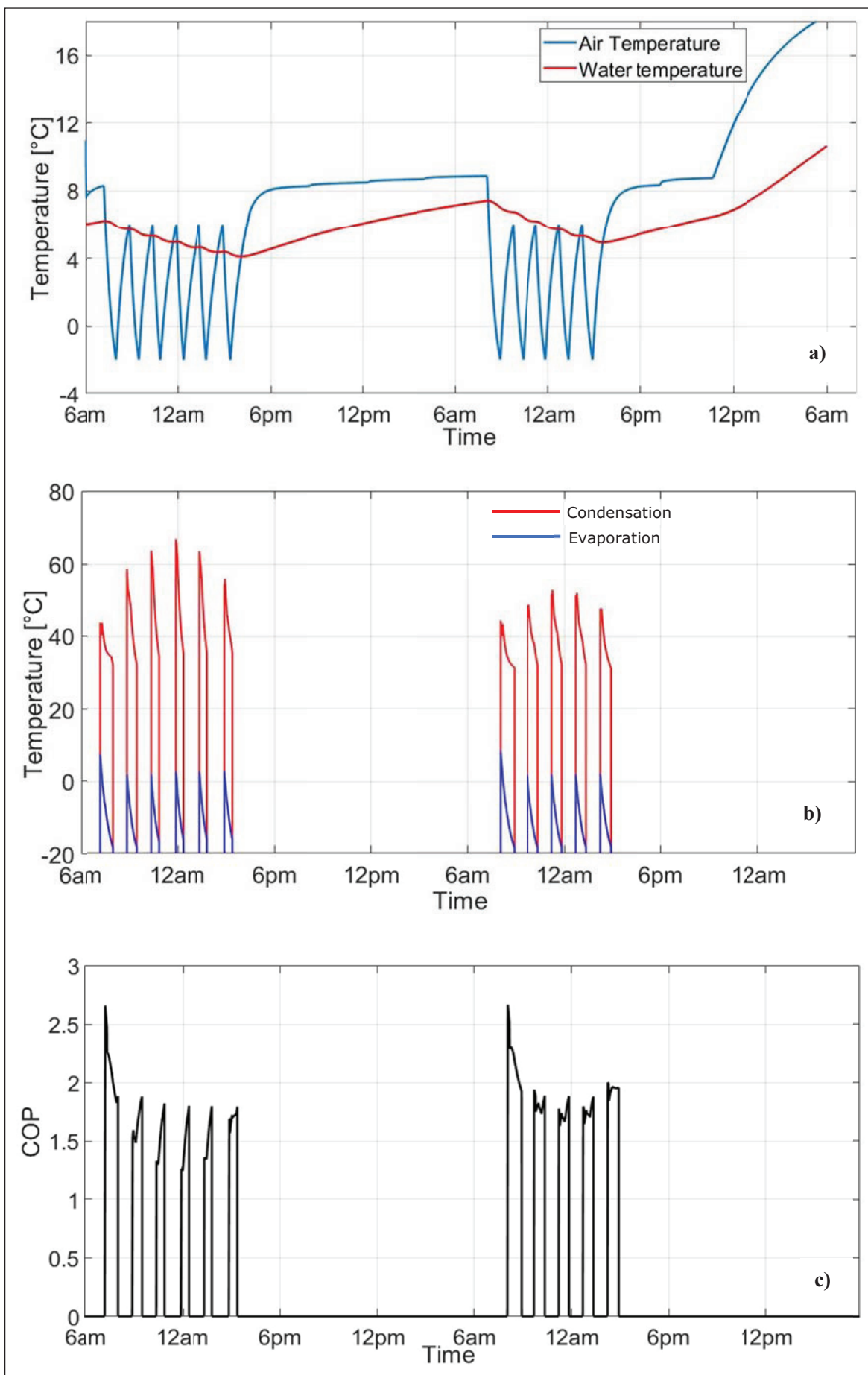


Figure 15: Variation of parameters during two days, water and air temperature (a), condensing and evaporation temperature (b), COP (c).

5. Conclusions

In this paper, a transient model is developed for a variable speed DC refrigerator for PV applications using phase change material as cold storage. A simplified differential equations model has been used to predict the impact of temperature setting, PCM addition and solar radiation levels. PV sourced PCM enhanced fridge performance metrics have been given in figures. As the main aim of the study is to increase the cold storage capacity of the fridge for rural applications, the PCMs provide enough cold storage for two days of electricity cut period. This will provide enough time to maintain foods in the fridge without spoilage. Since the study simulated a conventional fridge operation, the thermostat setting temperatures control the compressor on-off mode. When power production from the PV is higher than the consumption or during the compressor off time, the excess power can be transformed into AC power and feed the weak grid. Moreover, the following findings can be drawn:

- Initial CFD study showed that heat transfer coefficient between cold air and the PCM slabs inside the cabinet change between 3.9 and 4.8 W/m²K. The heat transfer coefficient was calculated considering average PCM surface temperature and average air temperature in the cabinet.
- The proposed study showed that variable speed DC compressor can operate sufficient refrigeration even in low solar radiation days, however, low solar radiation days reduce the PCM latent heat level because of late compressor starting time and early ending with weak solar intensity.
- Instant cooling load was found lesser in the low solar radiation day; thus, the compressor operates longer time in each compressor-on period to reduce fridge temperature to the setting temperature. Normally this longer cooling time would be an advantage for PCM charging, however, in the days of low solar radiation, number of compressor on-off times are also less than the normal days.
- Average COP of the system was found 1.7 for high solar days due to high rotation speed of the compressor, and 1.95 for low solar days due to lower compressor rotation speed.
- It was found that the unit can keep foods at the desired temperature range for two days of electricity cut period by using 1 m² PV collector and 3.6 kg of thin PCM packs.

Abbreviations

Nomenclature

<i>A</i>	Area, m ²
<i>c</i>	Specific heat, J kg ⁻¹ K ⁻¹
<i>D</i>	Diameter, m
<i>G</i>	Solar irradiance, W m ⁻²
<i>h</i>	Heat transfer coefficient, W m ⁻² K ⁻¹
<i>he</i>	Specific enthalpy, J/kg
ΔH_e	Enthalpy due to latent heat, J/kg
<i>k</i>	Thermal conductivity, W m ⁻¹ K ⁻¹
<i>Lat</i>	Latent heat of fusion, J/kg
<i>m</i>	Mass flow rate, kg s ⁻¹

<i>M</i>	Mass, kg
<i>N</i>	Rotation speed, Hz
<i>P</i>	Pressure, Pa
<i>Pr</i>	Prandtl number
\dot{Q}	Heat rate, W
<i>Re</i>	Reynolds number
<i>T</i>	Temperature, °C
<i>U</i>	Overall heat transfer coefficient, W m ⁻² K ⁻¹

Greek letters

η	Efficiency
η_v	Volumetric efficiency
ρ	Density, kg m ⁻³
λ	PCM liquid fraction

Subscripts

<i>a</i>	Ambient
<i>air</i>	Air inside the fridge
<i>b</i>	Boiling
<i>cap</i>	Capillary
<i>con</i>	Condenser
<i>ev</i>	Evaporator
<i>r</i>	Refrigerant
<i>ref</i>	Reference
<i>l</i>	Liquid
<i>v</i>	vapour
<i>tm</i>	Thermal mass
<i>tm-air</i>	Thermal mass to air

Acknowledgements

The authors would like to thank Efficiency for Access (EforA) for funding the project (RD2009) and also thank our partners PCM Products Ltd and Institute of Industrial Research for supporting this project.

Competing Interests

Saffa Riffat is the Editor in Chief of the journal and was removed from all editorial processing for this paper.

References

- Alrwashdeh, SS and Ammari, H.** 2019. Life Cycle Cost Analysis of Two Different Refrigeration Systems Powered by Solar Energy. *Case Studies in Thermal Engineering* 16 (August): 100559. DOI: <https://doi.org/10.1016/j.csite.2019.100559>
- Azzouz, K, Leducq, D and Gobin, D.** 2009. Enhancing the Performance of Household Refrigerators with Latent Heat Storage: An Experimental Investigation. *International Journal of Refrigeration*, 32(7): 1634–44. DOI: <https://doi.org/10.1016/j.ijrefrig.2009.03.012>
- Borges, B, Christian, H, Claudio, M and Joaquim, MG.** 2010. Transient Simulation of Household Refrigerators: A Semi-Empirical, Quasi-Steady Approach. *International Refrigeration and Air Conditioning Conference*.
- Breen, A, Sophie, B, Katrina, C, Mary, D, Gavin, D, Lucy, G and Sophie, L.** 2006. The Refrigerator Safari: An Educational Tool for Undergraduate Students Learning about the Microbiological Safety of Food. *British Food Journal*, 108(6): 487–94. DOI: <https://doi.org/10.1108/00070700610668450>

- Daffallah, KO.** 2018. Experimental Study of 12V and 24V Photovoltaic DC Refrigerator at Different Operating Conditions. *Physica B: Condensed Matter*, 545(May): 237–44. DOI: <https://doi.org/10.1016/j.physb.2018.06.027>
- Desideri, U, Stefania, P and Paolo, S.** 2009. Solar-Powered Cooling Systems: Technical and Economic Analysis on Industrial Refrigeration and Air-Conditioning Applications. *Applied Energy*, 86(9): 1376–86. DOI: <https://doi.org/10.1016/j.apenergy.2009.01.011>
- Du, K, Calautit, J, Wang, Z, Wu, Y and Liu, H.** 2018. A Review of the Applications of Phase Change Materials in Cooling, Heating and Power Generation in Different Temperature Ranges. *Applied Energy*, 220(October 2017): 242–73. DOI: <https://doi.org/10.1016/j.apenergy.2018.03.005>
- El-Bahloul, AAM, Ali, AHH and Shinichi, O.** 2015. Performance and Sizing of Solar Driven Dc Motor Vapor Compression Refrigerator with Thermal Storage in Hot Arid Remote Areas. *Energy Procedia*, 70: 634–43. DOI: <https://doi.org/10.1016/j.egypro.2015.02.171>
- Elarem, R, Mellouli, S, Abhilash, E and Jemni, A.** 2017. Performance Analysis of a Household Refrigerator Integrating a PCM Heat Exchanger. *Applied Thermal Engineering*, 125: 1320–33. DOI: <https://doi.org/10.1016/j.applthermaleng.2017.07.113>
- Gao, Y, Ji, J, Han, K and Zhang, F.** 2021. Comparative Analysis on Performance of PV Direct-Driven Refrigeration System under Two Control Methods. *International Journal of Refrigeration*. DOI: <https://doi.org/10.1016/j.ijrefrig.2021.03.003>
- Geete, P, Singh, HP and Somani, SK.** 2018. Performance Analysis by Implementation of Microencapsulated PCM in Domestic Refrigerator: A Novel Approach. *International Journal of Applied Engineering Research*, 13(19): 14365–71.
- Ghahramani Zarajabad, O and Ahmadi, R.** 2018. Numerical Investigation of Different PCM Volume on Cold Thermal Energy Storage System. *Journal of Energy Storage*, 17(February): 515–24. DOI: <https://doi.org/10.1016/j.est.2018.04.013>
- Hundy, GF.** 2016. *Refrigeration, Air Conditioning and Heat Pumps*. 5th ed. Butterworth-Heinemann. DOI: <https://doi.org/10.1016/B978-0-08-100647-4.00003-6>
- International Energy Agency IEA.** 2019. World Energy Outlook 2019. 2019. <https://www.iea.org/data-and-statistics/charts/people-without-access-to-electricity-worldwide-2000-2016>.
- James, SJ, Evans, J and James, C.** 2008. A Review of the Performance of Domestic Refrigerators. *International Journal of Refrigeration*, 87: 2–10. DOI: <https://doi.org/10.1016/j.jfoodeng.2007.03.032>
- Jung, D, Park, C and Park, B.** 1999. Capillary Tube Selection for HCFC22 Alternatives. *Lection de Capillaires Pour Les Frigorige A Nes de Remplacement Se.* 22: 604–14. DOI: [https://doi.org/10.1016/S0140-7007\(99\)00027-4](https://doi.org/10.1016/S0140-7007(99)00027-4)
- Karthikeyan, A, Sivan, VA, Khaliq, AM and Anderson, A.** 2020. Performance Improvement of Vapour Compression Refrigeration System Using Different Phase Changing Materials. *Materials Today: Proceedings*, no. xxxx: 3–6. DOI: <https://doi.org/10.1016/j.matpr.2020.09.296>
- Kumar, M and Kumar, A.** 2017. Performance Assessment and Degradation Analysis of Solar Photovoltaic Technologies: A Review. *Renewable and Sustainable Energy Reviews*, 78(November 2016): 554–87. DOI: <https://doi.org/10.1016/j.rser.2017.04.083>
- Kutlu, C, Tahir, M, Li, J, Wang, Y and Su, Y.** 2019. A Study on Heat Storage Sizing and Flow Control for a Domestic Scale Solar-Powered Organic Rankine Cycle-Vapour Compression Refrigeration System. *Renewable Energy*, 143: 301–12. DOI: <https://doi.org/10.1016/j.renene.2019.05.017>
- Kutlu, C, Zhang, Y, Elmer, T, Su, Y and Riffat, S.** 2020. A Simulation Study on Performance Improvement of Solar Assisted Heat Pump Hot Water System by Novel Controllable Crystallization of Supercooled PCMs. *Renewable Energy*, 152: 601–12. DOI: <https://doi.org/10.1016/j.renene.2020.01.090>
- Lamberg, P, Lehtiniemi, R and Henell, AM.** 2004. Numerical and Experimental Investigation of Melting and Freezing Processes in Phase Change Material Storage. *International Journal of Thermal Sciences*, 43(3): 277–87. DOI: <https://doi.org/10.1016/j.ijthermalsci.2003.07.001>
- Mahdi, MS, Mahood, HB, Mahdi, JM, Khadom, AA and Campbell, AN.** 2020. Improved PCM Melting in a Thermal Energy Storage System of Double-Pipe Helical-Coil Tube. *Energy Conversion and Management*, 203(November 2019): 112238. DOI: <https://doi.org/10.1016/j.enconman.2019.112238>
- Manfrida, G, Secchi, R and Stańczyk, K.** 2016. Modeling and Simulation of Phase Change Material Latent Heat Storages Applied to a Solar-Powered Organic Rankine Cycle. *Applied Energy*, 179: 378–88. DOI: <https://doi.org/10.1016/j.apenergy.2016.06.135>
- Marques, AC, Davies, GF, Maidment, GG, Evans, JA, and Wood, ID.** 2014. Novel Design and Performance Enhancement of Domestic Refrigerators with Thermal Storage. *Applied Thermal Engineering*, 63(2): 511–19. DOI: <https://doi.org/10.1016/j.applthermaleng.2013.11.043>
- Mattei, M, Notton, G, Cristofari, C, Muselli, M and Poggi, P.** 2006. Calculation of the Polycrystalline PV Module Temperature Using a Simple Method of Energy Balance. *Renewable Energy*, 31(4): 553–67. DOI: <https://doi.org/10.1016/j.renene.2005.03.010>
- Omara, AAM and Mohammedali, AAM.** 2020. Thermal Management and Performance Enhancement of Domestic Refrigerators and Freezers via Phase Change Materials: A Review. *Innovative Food Science and Emerging Technologies*, 66(September): 102522. DOI: <https://doi.org/10.1016/j.ifset.2020.102522>
- Opoku, R, Anane, S, Edwin, IA, Adaramola, MS and Seidu, R.** 2016. Évaluation Comparative Technico-Économique d'un Réfrigérateur Converti à Courant Continu (DC) et d'un Réfrigérateur Conventionnel à Courant Alternatif (AC) Tous Alimentés Par Du Solaire Photovoltaïque (PV). *International*

Journal of Refrigeration, 72: 1–11. DOI: <https://doi.org/10.1016/j.ijrefrig.2016.08.014>

- Oró, E, Miró, L, Farid, MM and Cabeza, LF.** 2012. Thermal Analysis of a Low Temperature Storage Unit Using Phase Change Materials without Refrigeration System. *International Journal of Refrigeration*, 35(6): 1709–14. DOI: <https://doi.org/10.1016/j.ijrefrig.2012.05.004>
- Pavithran, A, Sharma, M and Shukla, AK.** 2020. An Investigation on the Effect of PCM Incorporation in Refrigerator through CFD Simulation. *Materials Today: Proceedings*, no. xxxx. DOI: <https://doi.org/10.1016/j.matpr.2020.09.344>
- Phase Change Material Products.** n.d. Subzero PCMs List. Accessed December 7, 2020. <https://www.pcm-products.net/files/PCM Range 2020 Rev-B.pdf>
- PVGIS.** 2020. Photovoltaic Geographical Information System. EU Science Hub – European Commission. 2020. <https://ec.europa.eu/jrc/en/pvgis>
- Refrigerator.** n.d. Accessed January 18, 2020. <https://en.wikipedia.org/wiki/Refrigerator>
- Sabry, AH and Ker, PJ.** 2020. DC Environment for a Refrigerator with Variable Speed Compressor; Power Consumption Profile and Performance Comparison. *IEEE Access*, 8(Dc): 147973–82. DOI: <https://doi.org/10.1109/ACCESS.2020.3015579>
- Sajid, MU and Bicer, Y.** 2021. Comparative Life Cycle Cost Analysis of Various Solar Energy-Based Integrated Systems for Self-Sufficient Greenhouses. *Sustainable Production and Consumption*, 27: 141–56. DOI: <https://doi.org/10.1016/j.spc.2020.10.025>
- Salilih, EM and Birhane, YT.** 2019. Modelling and Performance Analysis of Directly Coupled Vapor Compression Solar Refrigeration System. *Solar Energy*, 190(July): 228–38. DOI: <https://doi.org/10.1016/j.solener.2019.08.017>
- Santiago, I, Trillo-Montero, D, Moreno-Garcia, IM, Pallarés-López, V and Luna-Rodríguez, JJ.** 2018. Modeling of Photovoltaic Cell Temperature Losses: A Review and a Practice Case in South Spain. *Renewable and Sustainable Energy Reviews*, 90(June 2017): 70–89. DOI: <https://doi.org/10.1016/j.rser.2018.03.054>
- Sharma, A.** 2011. A Comprehensive Study of Solar Power in India and World. *Renewable and Sustainable Energy Reviews*, 15(4): 1767–76. DOI: <https://doi.org/10.1016/j.rser.2010.12.017>
- Sonnenrein, G, Elsner, A, Baumhögger, E, Morbach, A, Fieback, K and Vrabec, J.** 2015. Reducing the Power Consumption of Household Refrigerators through the Integration of Latent Heat Storage Elements in Wire-and-Tube Condensers. *International Journal of Refrigeration*, 51: 154–60. DOI: <https://doi.org/10.1016/j.ijrefrig.2014.12.011>
- Su, P, Ji, J, Cai, J, Gao, Y and Han, K.** 2020. Dynamic Simulation and Experimental Study of a Variable Speed Photovoltaic DC Refrigerator. *Renewable Energy*, 152: 155–64. DOI: <https://doi.org/10.1016/j.renene.2020.01.047>
- Sun, L and Mishima, K.** 2009. An Evaluation of Prediction Methods for Saturated Flow Boiling Heat Transfer in Mini-Channels. *International Journal of Heat and Mass Transfer*, 52(23–24): 5323–29. DOI: <https://doi.org/10.1016/j.ijheatmasstransfer.2009.06.041>
- World Bank.** 2019. Data World Bank. Data by Country. 2019. https://data.worldbank.org/indicator/IC.ELC.OUTG?end=2020&name_desc=true&start=2006&view=chart
- Yilmaz, D, Mancuhan, E and Yilmaz, B.** 2020. Experimental Investigation of PCM Location in a Commercial Display Cabinet Cooled by a Transcritical CO₂ System. *International Journal of Refrigeration*, 120: 396–405. DOI: <https://doi.org/10.1016/j.ijrefrig.2020.09.006>
- Zubi, G, Dufo-López, R, Pasaoglu, G and Pardo, N.** 2016. Techno-Economic Assessment of an off-Grid PV System for Developing Regions to Provide Electricity for Basic Domestic Needs: A 2020–2040 Scenario. *Applied Energy*, 176(2016): 309–19. DOI: <https://doi.org/10.1016/j.apenergy.2016.05.022>

How to cite this article: Riffat, J, Kutlu, C, Brito, ET, Su, Y and Riffat, S. 2021. Performance Analysis of a PV Powered Variable Speed DC Fridge Integrated with PCM for Weak/Off-Grid Setting Areas. *Future Cities and Environment*, 7(1): 6, 1–18. DOI: <https://doi.org/10.5334/fce.121>

Submitted: 18 March 2021

Accepted: 20 May 2021

Published: 09 June 2021

Copyright: © 2021 The Author(s). This is an open-access article distributed under the terms of the Creative Commons Attribution 4.0 International License (CC-BY 4.0), which permits unrestricted use, distribution, and reproduction in any medium, provided the original author and source are credited. See <http://creativecommons.org/licenses/by/4.0/>.

][

Future Cities and Environment, is a peer-reviewed open access journal published by Ubiquity Press.

OPEN ACCESS 